Journal of Nonlinear Optical Physics & Materials
Vol. 8, No. 1 (1999) 1–20

NONLINEAR OPTICAL PROPAGATION PHENOMENA IN NEAR-TRANSITION CENTROSYMMETRIC PHOTOREFRACTIVE CRYSTALS

E. DELRE
Fondazione Ugo Bordoni, Via B. Castiglione 59, 00142 Rome, Italy

A. CIATTONI, B. CROSIGNANI* and P. DI PORTO
Università dell'Aquila, 67010 L'Aquila, Italy and INFM, Sezione di Roma 1, Italy

Received 13 January 1999

We relate on a series of optical nonlinear propagation phenomena, mediated by photorefraction, present in ferroelectric crystals heated above the Curie point, in proximity of the critical regime. In particular, we discuss centrosymmetric screening solitons, diffusion-driven anisotropic nonlinear diffraction, ellipticity locking, diffusion-driven solitons, and spatial beam head-on collisions.

1. Introduction

According to our present understanding, robust, undistorted, propagation of highly confined perturbations in dispersive continuos media, otherwise termed *solitons* or *solitary waves*, develop from a nonlinear host-perturbation interaction that ultimately compensates dispersion.[1] In Optics, solitons are generally identified with propagation of ultrashort pulses that do not suffer dispersion, known as *temporal solitons*,[2] and spatially confined optical beams that do not undergo diffraction, known as *spatial solitons*.[3] Limiting our discussion to this last type of phenomena, we can intuitively imagine the formation of a spatial soliton as due to a self-induced waveguide, engendered, in the host medium, by a light-induced modulation of the index of refraction, mediated by some more or less complicated light-matter interaction. Spatial optical solitons have been observed in Kerr-like media, in quadratic media, and in photorefractives.[3] In particular, photorefractive crystals have recently attracted much attention due to the relative "ease" of observation, in these

*Corresponding Author: Prof. Bruno Crosignani, Istituto Nazionale Fisica della Materia, Dipartimento di Fisica, Università di Roma I, 00185 Roma, Italy
Phone: +390649913469, fax: +39064463158, E-mail: bruno.crosignani@aquila.infn.it

materials, of steady-state spatial solitons, in a simple electro-optic configuration: the "screening" nonlinearity.[4] The resulting photorefractive self-trapped beams, engendered through the local screening of an external electric field via light-induced charges, have been employed in numerous basic configurations, allowing the experimental analysis of fundamental soliton properties and behaviors, and have rapidly extended the scope of nonlinear optical propagation to entirely new phenomena and circumstances. Thus, screening solitons have permitted the detection of stable two-dimensional soliton particles,[5] of soliton-soliton spiralling,[6] and of self-trapping of incoherent light beams.[7]

Since the discovery of spatial self-trapping in photorefractive media,[8] photorefractive solitons have been studied, theoretically and experimentally, in crystals in a stable *ferroelectric polar phase*.[4] In this phase, ferroelectrics manifest a strong spontaneous polarization along a particular axis (uniaxial structure) known as the optical axis, and the resulting electro-optic response is referred to as the linear electro-optic effect, characterized by a *linear* dependence of the local crystal index of refraction on the internal electric field.

Photorefraction, however, is not peculiar to this noncentrosymmetric phase.[9] Ferroelectrics are characterized by a number of different crystal states. The highest symmetry phase, in which all traces of spontaneous polarization disappear, generally referred to as the paraelectric phase, is characterized by a centrosymmetric crystal lattice and by a *quadratic* electro-optic response. Photorefraction, in this phase, is mediated by a light-induced index modulation that is proportional to the square of the induced internal electric field. Clearly, in the absence of spontaneous polarization, the electro-optic susceptibility is strongly diminished, and is similar to electrostriction (present in many nonferroelectric materials). Operating, on the other hand, in proximity of the polar phase-transition, at temperatures slightly above the Curie temperature T_c at which spontaneous polarization emerges, strongly enhances the low-frequency material response. Maintaining the crystal close to the transition point, on the dielectric anomaly, has actually allowed the observation of significant photorefractive effects.[10] Pioneering experiments, however, were hampered by one basic complication: the not easily accessible values of T_c. Initial paraelectric experiments were carried in KTN and KLTN at low values of T_c.[11] Recently, on the other hand, a particular composition of KLTN has allowed the realization of high quality bulk samples with *room temperature* ferroelectric-paraelectric phase transition.[10] This achievement has stimulated a renewed interest in the field, and opened up a variety of novel nonlinear optical propagation phenomena that are here discussed. In particular, photorefractive paraelectrics have been shown to support spatial centrosymmetric screening solitons,[12–14] that are qualitatively equivalent to their polar analogues. This means that most of the experiments carried out in the polar phase can be reproduced, *mutatis mutandis*, directly in the near-transition nonpolar phase. We shall here describe the experimental observation of these solitons both in the $1 + 1$D (one transverse and one propagation dimension)[13] and $2 + 1$D[14] cases. The story, however, does not end in this discovery. Polar crystals

support, in the steady-state, screening solitons[4] and photovoltaic solitons.[15] Recent investigation has shown that the nonpolar phase supports a somewhat different, varied, soliton phenomenology, such as for example, charge diffusion-driven nonlinear phenomena.[16,17] The main difference between the two regimes lies in the fact that the near-transition nonpolar regime brings into action a series of nonlinear material processes not relevant in the stable noncentrosymmetric phase, through the progressive enhancement of light-induced material changes in proximity of the dielectric anomaly. The strong influence of charge diffusion, the so-called photoferroelectric effect, static material nonlinear polarization, hysteresis etc. all can come to play a significant role near the transition, not to mention thermal effects and domain clustering and enucleation.[18] To date, there is strong evidence that these are present, but explicit investigation has only been carried out for diffusion-driven phenomena. In particular, we describe how the basic photorefractive model describes peculiar optical self-action, such as intensity independent self-focusing, and two-dimensional anisotropic effects, such as beam aspect-ratio locking. We furthermore discuss the prediction of an entirely new class of spatial solitons, both in $1+1$D and $2+1$D cases, with very peculiar and novel characteristics, known as diffusion-driven solitons. Diffusion-driven self-trapping permits, finally, the investigation of nonlinear phenomena in head-on collisions between confined counterpropagating beams, and we here describe a new approach to the theoretical description of such configurations, that are inherently characterized by strong nonlocality and nonlinear feedback.

In Sec. 2, centrosymmetric screening solitons are discussed, along with evidence of nonlinear material effects not contemplated in the simplified local quadratic screening model. In Sec. 3, the theoretical photorefractive model of beam propagation in a nonpolar ferroelectric in proximity of T_c, is described and solved, leading to nonlinear beam diffraction and diffusion-driven solitons. In Sec. 4, experimental evidence of diffusion-driven self-focusing is described, along with the observation of beam aspect-ratio locking. Both phenomena are directly interpreted by means of the diffusion-based model described in Sec. 3. In Sec. 5, head-on collisions of confined optical beams is discussed by means of a novel feedback approach.

2. Centrosymmetric Screening Solitons

Centrosymmetric screening solitons are supported by the same basic physical mechanism that gives rise to conventional noncentrosymmetric screening solitons, although mediated by the quadratic, rather than the linear, electro-optic effect. The resulting phenomenologies are quite similar, although direct comparison between theory and experiment reveals that nonlinear near-transition material mechanisms, not contemplated in the screening interaction, are playing an important, albeit as yet not clarified, role.

The essential process supporting screening solitons can be summarized, in the $1+1$D case, as follows (refer to Fig. 1): a highly confined optical beam is focused onto the input facet of a zero-cut photorefractive crystal and propagates along a

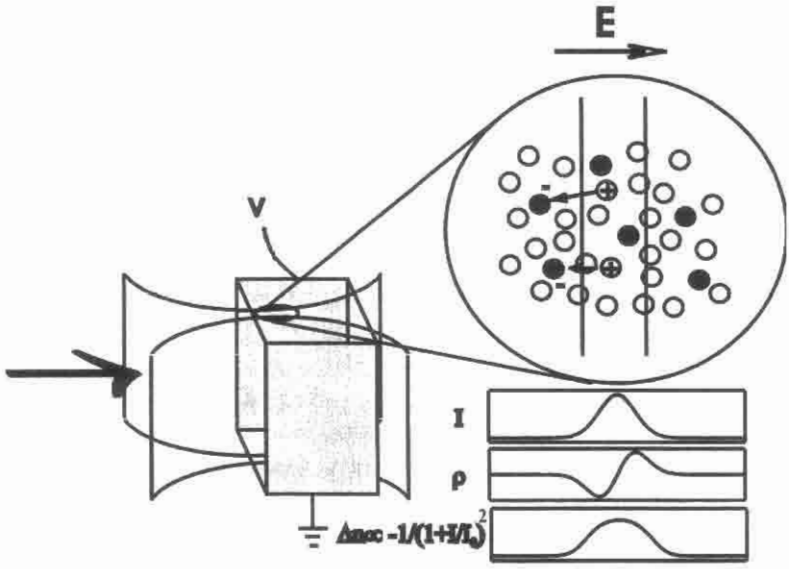

Fig. 1. Photorefractive screening mechanism.

crystal axis (for example, z). As the beam propagates in the material, it diffracts in the confined direction (say, the x dimension). The crystal, in itself transparent to the optical field (typically, the gap energy corresponds to optical wavelengths $\lambda <$ 300 nm), is characterized by a small amount of impurities that act as photosensitive donor sites. The beam excites conduction charges that are free to diffuse or drift in an external field. Neglecting, for the moment, charge diffusion (considered in the next sections), the application of an external field to the sample, parallel to the x axis, along which the beam suffers diffraction, displaces the charges so as to screen the resulting field in the illuminated region. This local modulation of electric field causes a corresponding local modulation of the index of refraction through the electro-optic response. When this modulation is such as to compensate diffraction, the self-induced lensing leads to self-focusing, and in particular conditions, to self-trapping.[19]

In the centrosymmetric case, the electro-optic change in index of refraction is proportional to the square of the polarization,[20]

$$(1/\Delta n)_{ij} = g_{ijkl} P_k P_1 \,, \tag{2.1}$$

where g_{ijkl} is the quadratic electro-optic tensor. Δn is expressed, in a scalar electro-optic configuration, by

$$\Delta n = -(1/2) n^3 g_{\text{eff}} \varepsilon_0^2 (\varepsilon_r - 1)^2 E^2 \,, \tag{2.2}$$

where E is the internal electric field, g_{eff} is the effective electro-optic coefficient, n is the crystal background index of refraction, $\varepsilon = \varepsilon_0 \varepsilon_r$ is the crystal dielectric

constant, and the material response is taken to be linear,

$$P = \varepsilon_0(\varepsilon_r - 1)E\,. \tag{2.3}$$

Typically, values of Δn obtained for reasonably accessible values of E (< 5 KV/cm) are far too low to support self-induced waveguiding (Δn has to be of the order of 10^{-4} to support a 10 μm optical soliton beam). Near the Curie point, however, the relative dielectric constant can take on values on the order of $\varepsilon_r \approx 10^4$, and self-trapping becomes feasible for relatively low applied voltages.

For materials with $g_{\text{eff}} > 0$, bright centrosymmetric 1+1D screening solitons can be shown to obey the local, saturated, and nonintegrable nonlinear wave equation[12]

$$\frac{d^2u(\xi)}{d\xi^2} = -\left[\frac{1}{1+u_0^2} - \frac{1}{(1+u^2(\xi))^2}\right] u(\xi)\,, \tag{2.4}$$

where $u(\xi)$ is the soliton amplitude normalized to the square root of the sum of background and dark irradiances, $\xi = x/d$ is the transverse coordinate normalized to the characteristic nonlinear length scale $d = (2kb)^{-1/2}$, with $b = (k/n)(1/2)n^3 g_{\text{eff}}\varepsilon_0^2$ $(\varepsilon_r - 1)^2(V/L)^2$, $k = 2\pi n/\lambda$, λ is the vacuum wavelength, V the applied voltage, and L is the width of the crystal between the opposite electrode faces (see Figs. 1 and 3).

Equation (2.4) does not have explicit analytical solutions. It does however, have non-analytical solutions in the form of self-trapped optical pulses. The actual solution can only be found numerically, and the resulting beam shape, analyzed elsewhere,[21] is somewhat similar to a Gaussian pulse. Numerical solutions of Eq. (2.4) form a set of parameter values in the $(u_0, \Delta\xi)$ plane, where u_0^2 is the ratio between the peak pulse intensity and the background illumination (intensity ratio), and $\Delta\xi$ is the normalized full-width-half-maximum (FWHM) of the pulse. The subspace corresponding to these soliton existence points is generally referred to as the "soliton existence curve." Equation (2.4), like its ferroelectric counterpart, tends to become a Kerr-like nonlinearity in the $u_0 \to 0$ limit.

We have previously underlined the critical importance of crystal temperature in centrosymmetric nonlinear phenomena, and in the simple screening model, proximity to transition *only* influences the value of the dielectric constant ε. In general, for most ferroelectrics, the static dielectric constant obeys, in the linear centrosymmetric phase (i.e., when Eq. (2.3) is valid), the Curie–Weiss phenomenological relationship

$$\varepsilon_r = \frac{C}{T - T_0}\,, \tag{2.5}$$

where C and T_0 are phenomenological constants. We have observed 1 + 1D solitons in a sample of bulk KLTN (potassium-lithium-tantalate-niobate), doped with Copper and Vanadium impurities. Measured values of low frequency (< 10 Kc/s) ε_r, through a standard capacitance measurement, are reported, for this particular crystal, as a function of temperature in Fig. 2. The crystal manifests a first-order displacive ferroelectric-paraelectric phase transition at $T_c \approx 12°$C, and has $C \cong 1.3 \times 10^5$ (°C) and $T_0 \cong 6.2°$C.

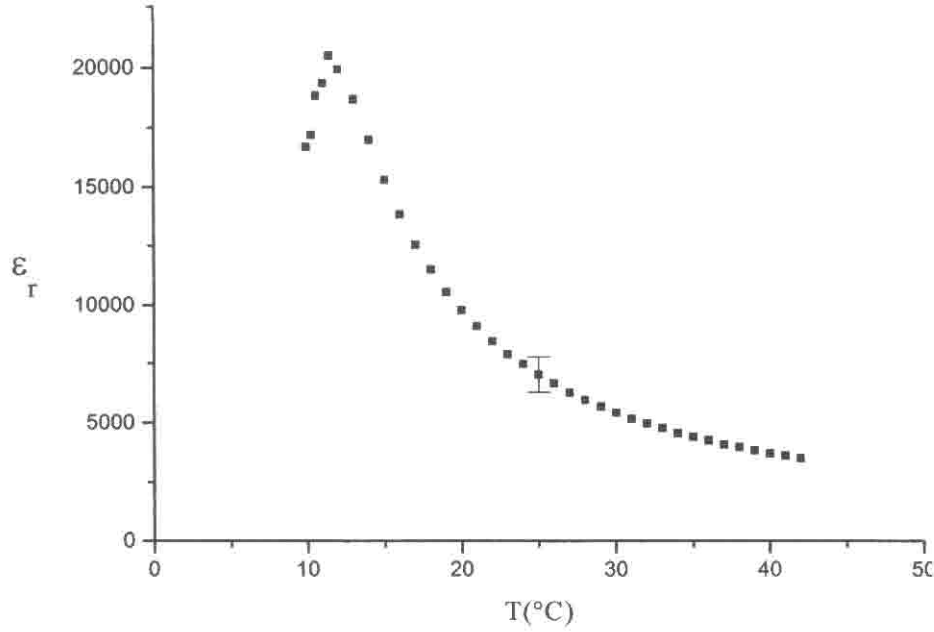

Fig. 2. Measured values of relative dielectric constant versus temperature for the sample of KLTN.

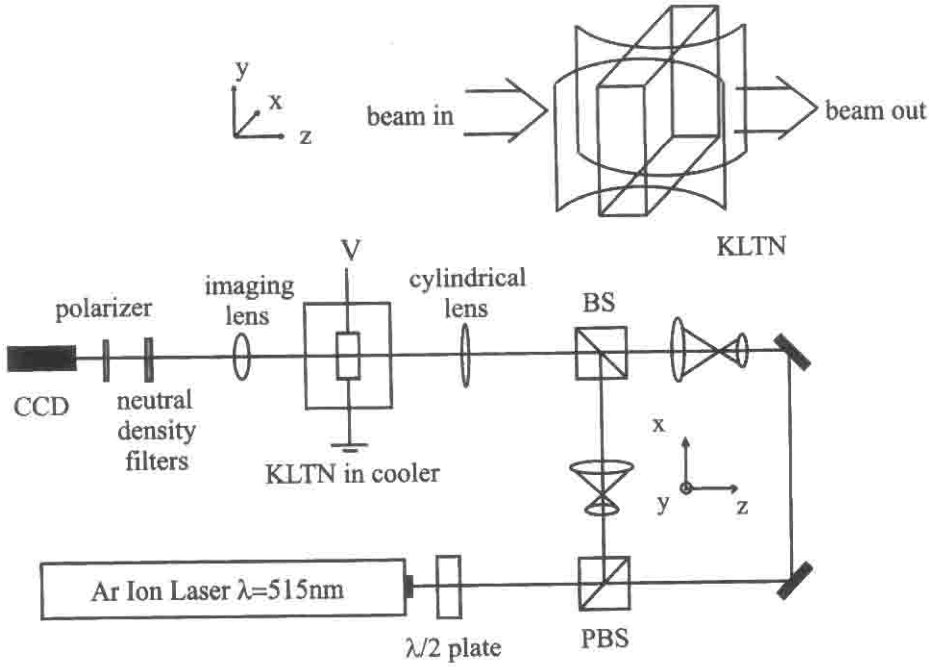

Fig. 3. Experimental configuration.

The experimental apparatus is shown in Fig. 3. A cw argon-ion laser beam is split into orthogonal polarizations by a polarizing beam splitter. The transmitted beam, polarized parallel to the plane (x-axis) of the figure, is focused by a cylindrical lens onto the input face of the KLTN sample, with its narrow direction parallel to x. The $3.7 \times 4.6 \times 2.4$ mm (in the x, y, z directions, where z is the propagation axis) crystal is kept at a constant temperature T by a current controlled Peltier junction. The g_{eff} for the x polarized beam, for an applied voltage V along the x axis, has a measured value of $g_{\text{eff}} \cong 0.12$ m^4 C^{-2}, and $n = 2.4$. Finally, the input and output crystal faces are imaged onto a CCD camera. The y polarized beam is used as the background artificial illumination.

Typical experimental results are shown in Fig. 4: a 9 μm FWHM 1+1D Gaussian beam diffracts to 29 μm with $V = 0$. For $V \cong 2$ KV, $T = 21°$C, and $u_0^2 = 2.9$, the beam self-traps, and no diffraction is observed.

In Fig. 5 we plot experimental existence points against the numerical theoretical existence curve. From this comparison to the simple screening theory two main things are evidenced. First of all, there is *good qualitative agreement*. This in contrast to the extreme simplicity of the screening model. Actual quantitative agreement is not demonstrated, as happens for all experiments with screening solitons in the ferroelectric phase.[19] The second, and perhaps more interesting observation, is that the existence curve, for two different crystal temperatures, *do not agree*. This last circumstance is believed to be due to the emergence of temperature dependent processes, such as local electric field-induced ε_r changes, that indicate the intrinsic limitations of the screening model, when in proximity of the transition.[22]

Amongst the many interesting aspects of spatial soliton physics connected to photorefractives, the existence of circular-symmetric self-trapped 2+1D beams is the

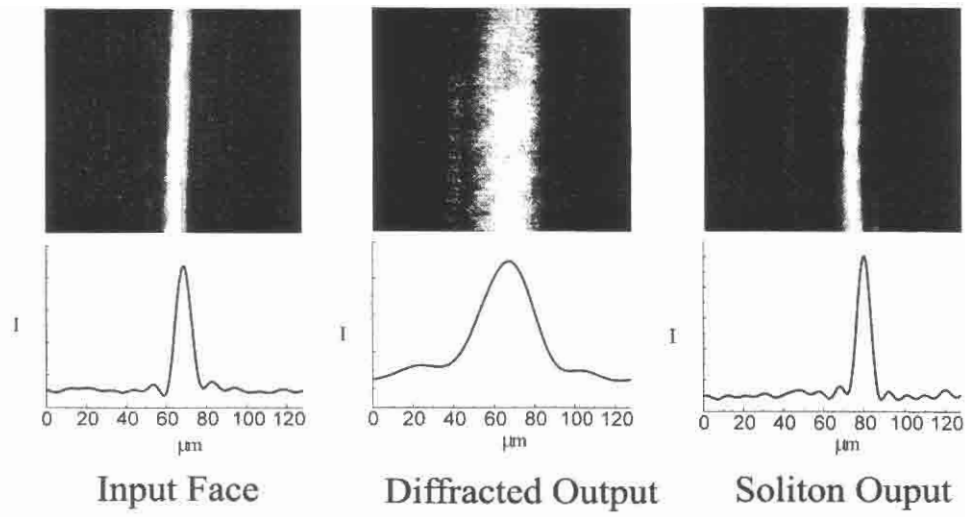

Fig. 4. Typical results for 1 + 1D screening solitons.

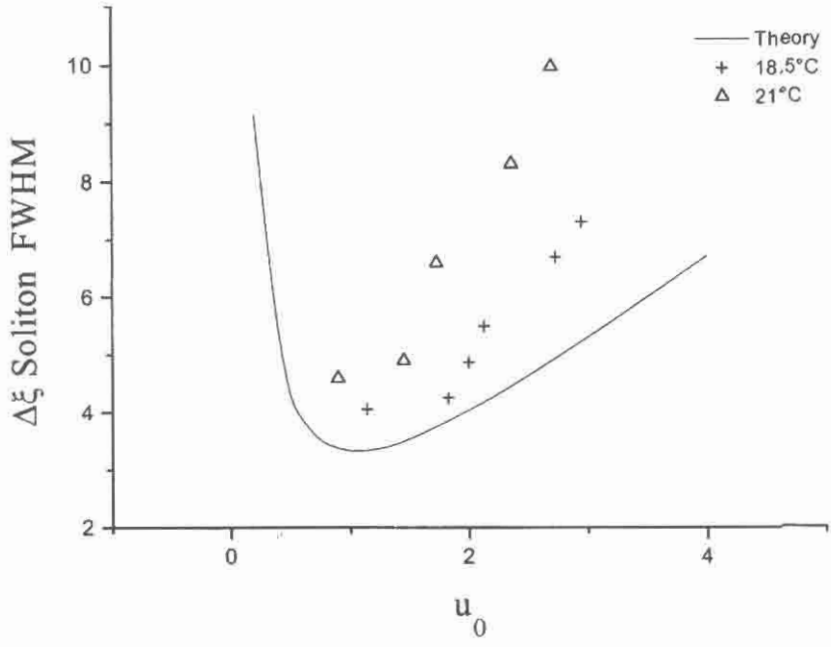

Fig. 5. Experimental soliton existence points compared to theory.

most debated.[5,23–25] Experiments in polar SBN (strontium-barium-niobate) have demonstrated the existence of stable circular screening solitons, although partial treatments of the full 2 + 1D screening model, not explicitly tractable, unlike the 1 + 1D case, seem to suggest that the strong anisotropy of the system could not possibly support such pulses. The actual solution of the dilemma is far from being solved, although recent investigations seem to identify in the influence of nonlocal components of the photorefractive interaction, a possible answer.[24,26]

Nonpolar KLTN supports 2 + 1D circular-symmetric centrosymmetric screening solitons, like SBN. Experiments have been carried out with the same apparatus illustrated in Fig. 3, with the cylindrical lens substituted with a spherical one. The sample of KLTN used was similar to the one previously described, except that it was longer (in the propagation direction), being $2.6 \times 1.8 \times 6.4$ mm (x, y, z directions), and thus allowed a more dramatic self-trapping phenomenology.

Typical experimental results are shown in Fig. 6, where an approximately circular-symmetric 7 μm intensity FWHM needle diffracts to 90 μm after propagating the entire 6.4 mm length of the sample. At $T = 29°\mathrm{C}$ ($T_c = 19°\mathrm{C}$ for this crystal) a voltage $V = 1.15$ KV is able to form a self-trapped 2 + 1D spatial soliton with $u_0^2 = 156$. The final trapped beam manifests a very slight anisotropy.

Although no theory is available to compare experimental 2 + 1D results, we are able to verify experimentally the presence of a 2 + 1D soliton existence curve, illustrated in Fig. 7.

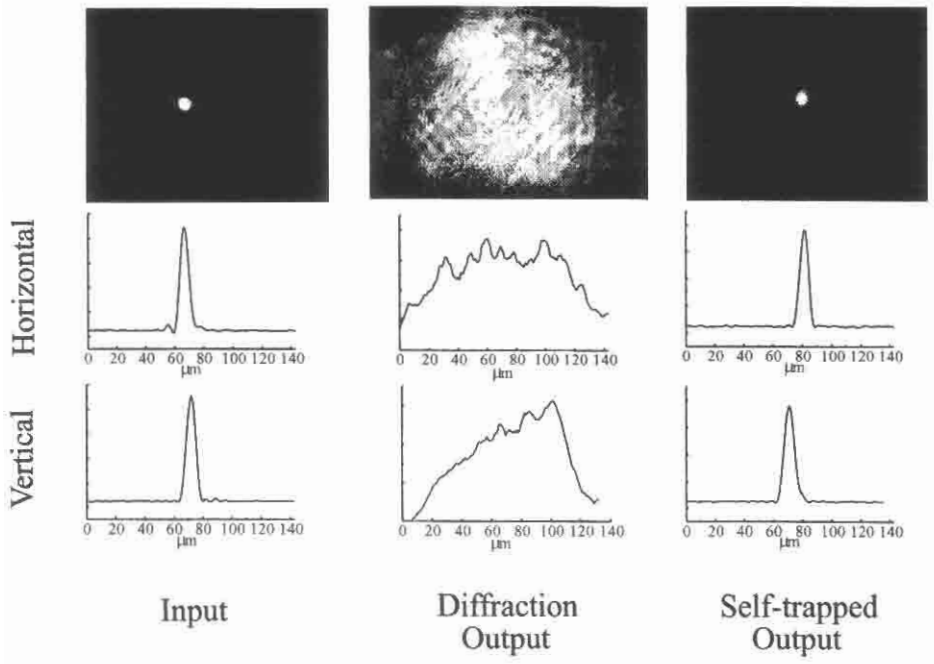

Fig. 6. Typical results for a 2 + 1D screening soliton.

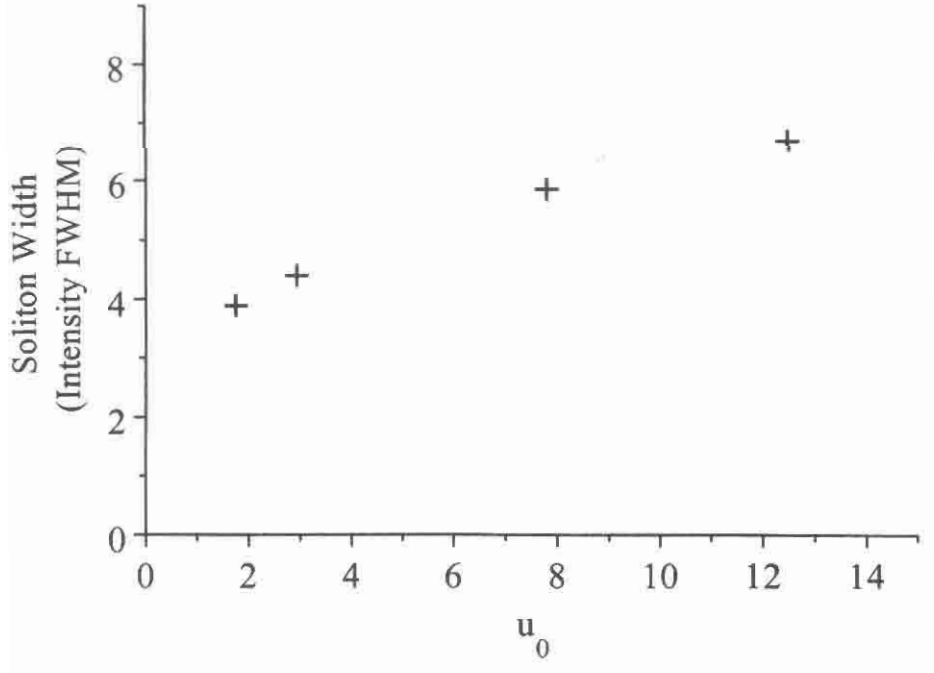

Fig. 7. Experimental 2 + 1D soliton existence points.

3. Analytic Description of Nonlinear Propagation in Unbiased Centro-Symmetric Photorefractive Media

We have previously discussed how the spatial structure of optical beams propagating in photorefractive crystals gives rise, through the process of photo-ionization of the donors present in the crystal, to an inhomogeneous spatial generation of free charges. In absence of an external field, these are redistributed by thermal diffusion and produce a space-charge separation and an electric field $\mathbf{E}$ (space-charge field) associated with this separation. The static field $\mathbf{E}$ modifies, through the Pockels' effect, the refractive index of the crystal. In order to determine the behavior of an optical beam propagating in a photorefractive crystal, one has first to express the space-charge field in terms of the optical intensity I and then, after connecting, through the Pockels' effect, the refractive index variation to the space-charge field, to solve the associated wave equation. Some drastic approximations (see, e.g. the cases of two-wave mixing and screening solitons) are in general required before arriving at some manageable wave equation (see, e.g. Ref. 27). Luckily, our specific problem requires only minor approximations and it is described by a remarkably simple wave equation, which admits of a wide class of analytic solutions.

We first derive the relationship between the space-charge field $\mathbf{E}$ and the optical intensity $I = |\mathbf{E}_{\rm op}|^2$, where $\mathbf{E}_{\rm op} = \mathbf{A}(x,y,z)\exp(ikz - i\omega t) + \text{c.c.}$ is the high-frequency optical field, $k = n\omega/c$ its wave-number, ω its frequency and n the linear refractive index of the medium (a scalar quantity, since we are dealing with centrosymmetric crystals) at the frequency ω. This is done by solving the differential equation relating $\mathbf{E}$ to I. This equation can be found in the frame of the so-called Kuchtarev model[28] and reads[27,29]

$$\tilde{\nabla}\cdot\left[\frac{\alpha-\tilde{\nabla}\cdot\mathbf{Y}}{1+\tilde{\nabla}\cdot\mathbf{Y}}Q\mathbf{Y}+\tilde{\nabla}\left(\frac{\alpha-\tilde{\nabla}\cdot\mathbf{Y}}{1+\tilde{\nabla}\cdot\mathbf{Y}}Q\right)\right]=0\,. \tag{3.1}$$

In Eq. (3.1), $\alpha = (N_D - N_A)/N_A$ (where N_A and N_D represent, respectively, the donor and acceptors density present in the dark inside the crystal) is typically much larger than one, $\mathbf{Y} = \mathbf{E}/E_d$ ($E_d = (K_B T/q\ell_D)$ being the so-called diffusion field), $\tilde{\nabla} \equiv (\partial/\partial\xi, \partial/\partial\eta, \partial/\partial\zeta)$ (with $(\xi,\eta,\zeta) = (x/\ell_D, y/\ell_D, z/\ell_D)$) and $\ell_D = (\varepsilon K_B T/q^2 N_A)^{1/2}$ is the Debye length (ε being the low-frequency dielectric constant of the crystal). Besides, we have defined $Q = 1 + |u|^2$, where $|u|^2 = I/I_b$ and I_b is the intensity associated with the dark conductivity of the crystal and a possible background illumination present in the crystal.

As a first approximation, we neglect in Eq. (3.1) the term $\tilde{\nabla}\cdot\mathbf{Y}$ with respect to one (and, *a fortiori*, with respect to α), thus getting

$$\tilde{\nabla}\cdot[QY + \tilde{\nabla}Q] = 0\,. \tag{3.2}$$

The solution of this equation, consistent with the boundary condition $I = 0$ on the

transverse faces of the crystal, reads

$$\mathbf{Y} = -\frac{\tilde{\nabla} Q}{Q}\,. \tag{3.3}$$

The approximation $\tilde{\nabla} \cdot \mathbf{Y} \ll 1$ has now to be checked *a posteriori* using Eq. (3.3). It is easy to see that it amounts to assuming $(\ell_D/\ell)|u|^2/(1+|u|^2) \ll 1$, where ℓ represents a typical scale of variation of the optical intensity I.

Having related, by means of Eq. (3.3), $\mathbf{E} = E_d \mathbf{Y}$ with the intensity I, we recall the expression of the refractive index change associated, through the Pockels' effect, with the presence of a given electrostatic field $\mathbf{E}$. Although, as discussed in Sec. 2, for near-transition operation, the main physical quantity of interest is the index modulation induced by a given polarization P, the quadratic Pockels' effect is generally introduced directly as a function of $\mathbf{E}$.[30] More precisely, if x, y, z are chosen along the principal axes of the crystal, its dielectric tensor ε_{ij} is given by

$$\varepsilon_{ij} = \varepsilon_0 n^2 (\delta_{ij} - n^4 r_{ijkm} E_k E_m), \quad (i,j = x,y,z) \tag{3.4}$$

where the tensor r_{ijkm} is responsible for the quadratic Pockels' effect.

The final step is to consider the parabolic wave equation which describes optical propagation in the paraxial approximation, i.e.,

$$\left(i\frac{\partial}{\partial z} + \frac{1}{2k}\nabla_\perp^2 \right) A_i(\mathbf{r}_\perp, z) + \frac{k}{n}\Delta n_{ij} A_j(\mathbf{r}_\perp, z) = 0\,, \tag{3.5}$$

where $\mathbf{r}_\perp = (x,y)$ and $\nabla_\perp^2 = (\partial^2/\partial x^2 + \partial^2/\partial y^2)$. Recalling Eqs. (3.3) and (3.4) and the definition of diffusion field E_d, Eq. (3.5) takes the form

$$\left(i\frac{\partial}{\partial z} + \frac{1}{2k}\nabla_\perp^2 \right) A_i - \frac{n^2}{2}(K_B T/q)^2 r_{ijkm} \left(\frac{\partial}{\partial x_k} \ln Q \frac{\partial}{\partial x_m} \ln Q \right) A_j = 0\,. \tag{3.6}$$

As mentioned, since the material response in the near-transition regime is connected to the induced polarization at a given temperature, in order to highlight the physics at the basis of the process, the nonlinear term in Eq. (3.6) can be rewritten in a slightly different form by recalling that the Pockels' effect is induced by the stationary polarization $\boldsymbol{P}$ (see Eq. (2.1)) and thus depends on the low-frequency dielectric constant ε. When Eq. (2.2) is valid, Eq. (3.6) can be recast in the form

$$\left(i\frac{\partial}{\partial z} + \frac{1}{2k}\nabla_\perp^2 \right) A_i - \frac{n^2}{2}(K_B T/q)^2 \varepsilon_0^2 (\varepsilon_r - 1)^2 g_{ijkm} \left(\frac{\partial}{\partial x_k} \ln Q \frac{\partial}{\partial x_m} \ln Q \right) A_j = 0\,. \tag{3.7}$$

Note that while far from the phase transition the tensor r_{ijkm} represents a convenient electro-optic quantity since it relates directly the electric field to the refractive index change, close to the phase transition it becomes strongly temperature dependent; conversely, the electro-optic tensor g_{ijkm} is approximately constant with the temperature.

Equation (3.7) can assume a scalar form if only two relevant electro-optic coefficients, that is $g_{xxxx} = g_{11} > 0$ and $g_{xxyy} = g_{12} > 0$, are nonzero. In this case, a linearly x-polarized input field remains x-polarized and its amplitude obeys the scalar wave-equation

$$\left(i\frac{\partial}{\partial Z} + \hat{\nabla}_\perp^2\right) u + \left(\gamma_1 \left(\frac{\partial |u|^2/\partial X}{|u|^2+1}\right)^2 + \gamma_2 \left(\frac{\partial |u|^2/\partial Y}{|u|^2+1}\right)^2\right) u = 0\,, \tag{3.8}$$

where $u = A_x/(I_b)^{1/2}, (X,Y) = 2^{1/2}(kx, ky)$, $Z = kz$, $\hat{\nabla}_\perp^2 = \partial^2/\partial X^2 + \partial^2/\partial Y^2$ and $\gamma_1 = -k^2 n^2 \varepsilon_0^2 (\varepsilon_r - 1)^2 g_{11} (K_B T/q)^2$, $\gamma_2 = -k^2 n^2 \varepsilon_0^2 (\varepsilon_r - 1)^2 g_{12} (K_B T/q)^2$.

If we neglect I_b with respect to the peak intensity I_0, that is neglect the influence of the beam tails (a circumstance which can be justified *a posteriori* comparing the exact analytical results with numerical ones), Eq. (3.8) takes the final form

$$\left(i\frac{\partial}{\partial Z} + \hat{\nabla}_\perp^2\right) u + \left(\gamma_1 \left(\frac{\partial |u|^2/\partial X}{|u|^2}\right)^2 + \gamma_2 \left(\frac{\partial |u|^2/\partial Y}{|u|^2}\right)^2\right) u = 0\,. \tag{3.9}$$

It is remarkable that nonlinear propagation in the presence of the diffusive nonlinearity associated with the quadratic electro-optic effect is described by such a simple equation. Still more remarkable is the fact that, unlike any other realistic nonlinearity (including the Kerr one), the resulting equation admits of a large variety of exact analytical solutions corresponding to nonlinear self-focused and trapped propagation.[16,17]

A class of self-focused solutions, valid for $0 > \gamma_{1,2} > -1/4$, has the Gaussian-like form

$$\mathbf{u} = \frac{\mathbf{u}_0}{(p_1 p_2)^{1/4}} \exp(-\xi^2/d_1^2 p_1 - \eta^2/d_2^2 p_2) \exp[i\phi(\xi,\eta,\zeta)]\,, \tag{3.10}$$

where $\mathbf{u}_0$ is a constant, d_1, d_2 are the (dimensionless) input widths in the x and y directions,

$$p_{1,2} = \left[1 + \frac{16(1+4\gamma_{1,2})}{d_{1,2}^4}(\zeta - \zeta_{1,2})^2\right], \tag{3.11}$$

$$\begin{aligned}\phi(\xi,\eta,\zeta) = {} & (p_1'\xi^2/p_1 + p_2'\eta^2/p_2)/8 - (2/d_1^2 b_1^{1/2}) tg^{-1}[b_1^{1/2}(\zeta - \zeta_1)] \\ & + (2/d_2^2 b_2^{1/2}) tg^{-1}[b_2^{1/2}(\zeta - \zeta_2)]\,,\end{aligned} \tag{3.12}$$

where $b_{1,2} = 16(1+4\gamma_{1,2})/d_{1,2}^4$ and the prime stands for derivative with respect to ζ.

The second class of solutions, valid for $\gamma_{1,2} < -1/4$, represents a class of non-Gaussian self-trapped solutions in the form of noncircular spatial solitons which read

$$\mathbf{u} = \mathbf{u}_0 \exp[-i(\alpha_1^2\beta_1^2 + \alpha_2^2\beta_2^2)] \cosh^{-\alpha_1^2}(\beta_1\xi) \cosh^{-\alpha_2^2}(\beta_2\eta)\,, \tag{3.13}$$

where $\alpha_1^2 = -1/(1+4\gamma_1)$, $\alpha_2^2 = -1/(1+4\gamma_2)$ and $\beta_{1,2}$ are arbitrary parameters (dependent on the input beam shape).

4. Experimental Observation of Diffusion-Driven Self-Focusing and Ellipticity Locking in Near-Transition KLTN

In the previous section we have shown how the basic photorefractive model allows the analytical prediction of a set of nonlinear propagation phenomena that ultimately lead to $2+1$D spatial solitons of *arbitrary* transverse beam-aspect ratio. Here we relate on experiments carried in a sample of KLTN, that partially confirm these theoretical predictions.

The experimental apparatus resembles the one illustrated in Fig. 3, however somewhat simplified. No background illumination is implemented (actually, background illumination plays a wholly marginal role, as previously discussed), and no external voltage V is used. The only addition to the scheme is a prism inserted before the focusing lens, in the $2+1$D case, that allows us to obtain, from the initial TEMoo laser beam, a tunable, approximately stigmatic noncircular Gaussian beam with a given ellipticity $\Lambda = FWHM_y/FWHM_x$.

The first experiment we performed consisted in launching into the sample of KLTN a 1D Gaussian beam and observing its diffraction at the output facet. The input beam, again a TEM_{00} $\lambda = 515$ nm polarized (along the x direction) beam from a CW Argon ion laser, is focused onto the input facet of the sample by means of a cylindrical lens with $f = 150$ mm (and axis parallel to the y direction). The input light distribution (a slab of light) has an input $FWHM$ of 13 μm (in the confined x direction). When the crystal is kept at room temperature ($T = 20°$C)

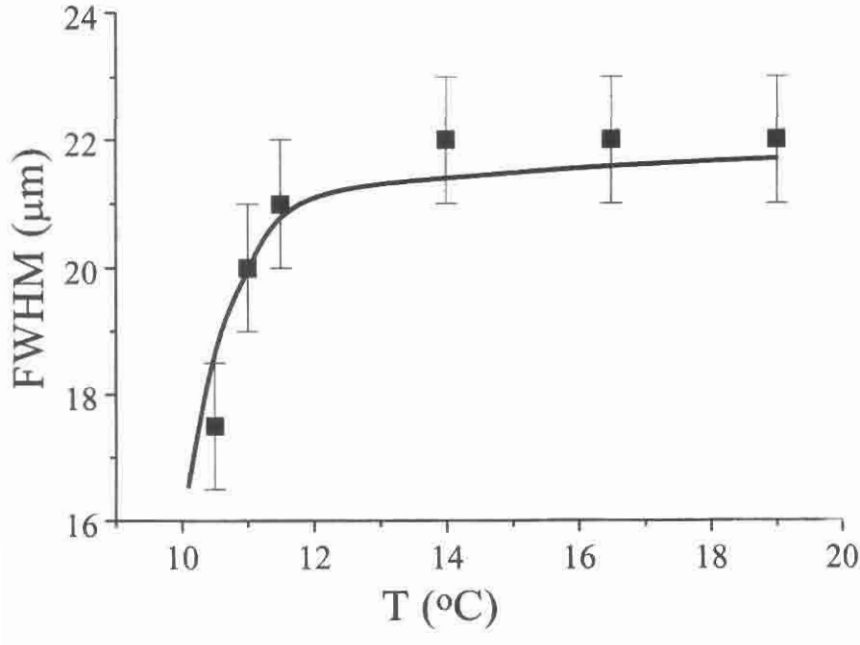

Fig. 8. $1+1$D diffusion-driven self-focusing.

the beam diffracts to 22 μm, as expected from linear Gaussian diffraction. Lowering the crystal temperature towards T_c we observed considerable self-focusing as shown in Fig. 8 from 22 μm to 17 μm. At even lower temperatures, as the critical regime was reached, we observed domain formation and strong beam distortion (first domain enucleation was observed at 10.0–10.2°C). Heat transfer occurred only through the bottom facet of the crystal which was therefore not uniformly thermalized during the experiment, presenting a transverse temperature gradient (especially at low values of T). Our observations refer to a limited transverse (in the xy plane) region of the crystal (about 200 × 200 μm) where the effect of the gradient was negligible. The peak beam intensity used was of the order of $I_0 \approx 10^2$ W/cm^2, at the crystal input face (spurious background illumination was at least four orders of magnitude less intense). The experiment was repeated for higher values of I_0 (up to ten times more intense), but no appreciable difference was observed, other than in the duration of the transient build-up regime.

Next we investigated 2 + 1D propagation. We substituted the cylindrical lens with a spherical one and launched at the input facet of the crystal a highly confined circular Gaussian beam. At the output we observed Gaussian linear propagation for room temperature, but as the crystal was cooled into the near-transition regime, we observed a peculiar beam deformation leading to a beam with elliptical transverse intensity profile. The beam manifested self-focusing in the x direction, parallel to the beam polarization (which did not suffer any rotation). Thus, introducing the prism, we launched an asymmetric elliptical, approximately stigmatic, Gaussian beam into the crystal and observed diffraction as a function of temperature. Results are shown in Fig. 9. The input beam, with intensity $FWHM_x = 7$ μm and $FWHM_y = 11$ μm, has an input ellipticity $\Lambda = (FWHM_y/FWHM_x) = 1.5$. For high values of temperature, at which beam propagation is linear (from approximately 15°C upwards diffusion has a negligible effect), we observed the typical "inversion" of ellipticity at the output of the crystal, from 1.5 to 0.7, this being a consequence of standard diffraction (stronger confinement, stronger diffraction). As we lowered the crystal temperature we observed an evolution of the output ellipticity towards a *higher value*. At approximately $T = 10.2$°C we recovered the input ellipticity, as shown in Fig. 9, the beam maintaining its Gaussian transverse profile. We adjusted the input laser power in order to have a peak intensity comparable to the 1 + 1D case and again repeated the experiment for various values of I_0 observing no appreciable difference in the final stationary configuration.

Qualitatively, both observed phenomena are directly described by the diffusion based theory described in Sec. 3. In order to test the quantitative agreement between theory and experiment we must evaluate the values of γ_1 (and γ_2) as a function of T. The beam astigmatism was negligible in the 2 + 1D configuration ($\zeta_1 = \zeta_2 = 0$). The principal dependence of the $\gamma_i (i = 1, 2)$ on temperature is through ε_r, that is greatly enhanced as the temperature is lowered towards T_c. In proximity of the phase-transition the bulk dielectric crystal response is smeared-out by the temperature gradient and other large-scale crystal inhomogeneities and values of ε_r will in general

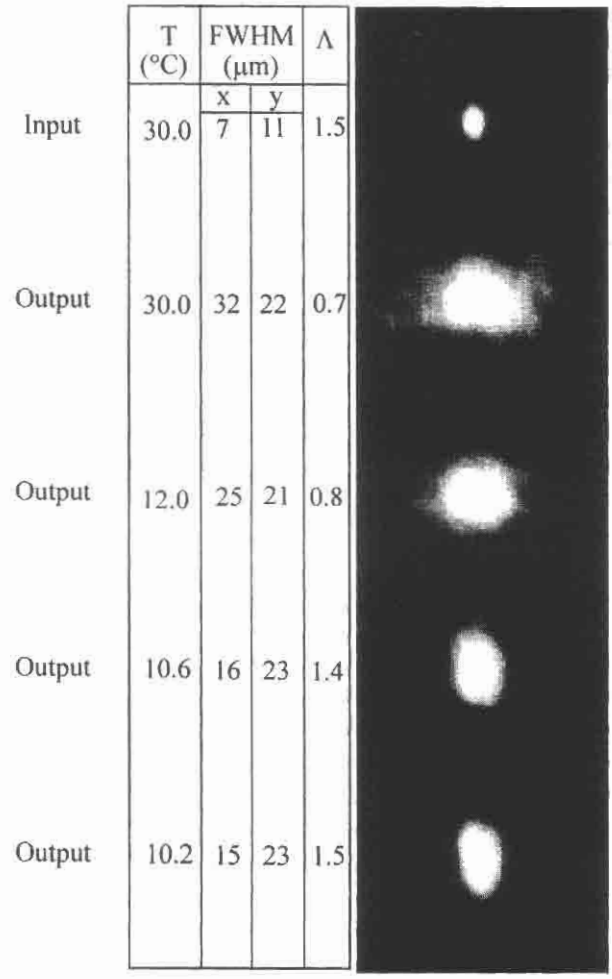

	T (°C)	FWHM (μm)		Λ
		x	y	
Input	30.0	7	11	1.5
Output	30.0	32	22	0.7
Output	12.0	25	21	0.8
Output	10.6	16	23	1.4
Output	10.2	15	23	1.5

Fig. 9. Ellipticity recovery driven by diffusion.

be far lower than actual "local" crystal values. For temperatures where these effects have a negligible effect ($T > 12°\mathrm{C}$ with our setup) we are able to fit bulk ε_r values with the Curie–Weiss law, as described in Sec. 2. The peak value of ε_r actually measured directly (in the capacitance experiment) was approximately 2×10^4 (see Fig. 2). For values of T closer to T_c we measured directly the local (for the transverse regions of about $200 \times 200\ \mu\mathrm{m}^2$) electro-optic index modulation by inserting the sample in one arm of a Mach–Zehnder interferometer. In the out-of-transition range, this allows also a measurement of $g_{11} = 0.12\ \mathrm{m}^4\ \mathrm{C}^{-2}$ and $g_{12} = 0.02\ \mathrm{m}^4\ \mathrm{C}^{-2}$ (having independently measured ε_r). The measured values[17] of γ_1 are higher than those expected from the Curie–Weiss relationship, and this can be phenomenologically attributed to an increase in the value of g_{11}, as the quadratic dependence of Δn still held for low applied voltages ($V < 250$ V). Values of γ_2 where such as to induce no

appreciable diffusion-driven effects, remaining its value always more than five times smaller (in absolute value) than the corresponding values of γ_1 for the temperatures investigated. In Fig. 8 the solid curve represents the theoretical curve obtained from Eqs. (3.10)–(3.11) with $d_2 \to \infty$. The quantitative agreement is satisfactory, although the strong focusing for temperatures very near T_c may indicate that here some different mechanism is playing an important role. For ellipticity recovery in the 2+1D case we recover the input ellipticity $\Lambda(0) = 1.5$ at $T = 10.2°C$ (see Fig. 9). From Eqs. (3.10)–(3.11) our theory predicts that the "recoverable" ellipticity at this temperature is $\Lambda_{\text{theor}} = 1.3$, being $\gamma_1 = -0.17$ and $|\gamma_2| \ll 1$. Thus again, as in the $1 + 1$D case, the nonlinear response is stronger than expected.

Regarding the possibility of observing noncircular diffusion-driven solitons, our samples of KLTN do not support a sufficiently strong dielectric anomaly. The mechanism is however not peculiar to KLTN and stronger anomalies have been reported in different ferroelectrics, such as SBN (strontium–barium–niobate) and SbSI (antimony sulphoiode).[18] In these materials at least $1 + 1$D solitons should be attainable.

5. Head-On Collisions of Confined Optical Beams

As discussed in Sec. 2, background illumination in noncentrosymmetric and centrosymmetric screening phenomena plays a central role. In diffusion-driven phenomena, on the contrary, background illumination can generally be neglected. This fact allows the direct investigation of slightly more complicated configurations such as head on collisions of two mutually incoherent light beams.

Consider two confined, counterpropagating light beams that suffer a collision inside a near-transition paraelectric. If the beams were coherent, they would give rise to counterpropagating two-wave-mixing and exchange energy.[28] Being mutually incoherent, the nonlinear interaction is of a more subtle and interesting sort, that can be synthetically described with the term "spatial nonlinear feedback." Intuitively, we can imagine the situation as follows: one beam propagates, diffracting, in the medium, engendering a diffusion-driven variation of the index of refraction that leads to its self-focusing, as described in Sec. 3. The second beam equally undergoes this process, "feeling," at the same time, the presence of the first beam through its index modulation, and vice versa. This mechanism leads to an optical feedback between the two beams. The configuration somewhat resembles optical feedback set-ups that have led to the observation, in photorefractives, of complex spatial structuring. In this case, however, emphasis is on spatial *dynamics* (not present in the typical plane-wave configuration).[31] This head-on configuration can have a very interesting application: consider two spatial solitons counterpropagating; if the solitons, mutually incoherent, are not in axis, they will tend to attract each other, and possibly coalesce, thus realizing a self-aligning component. The many interesting situations we can think of encounter one major obstacle: the complexity of theoretical description. The feedback system, in fact, naturally manifests nonlocality.

Propagation of a monochromatic paraxial beam, inside a medium possessing a small refractive index modulation, is correctly described by the parabolic wave-equation whose deduction from Helmholtz equation takes advantage of counter-propagating beam's absence.[32] Because here we are interested in studying counter-propagating beam interaction, a generalization of standard paraxial-approximation to the case of coexisting beams is fundamental. This issue is subtle, despite the simple result that we can actually write a parabolic equation for *each* single beam, the interaction being described by the refractive index dependence on the *total* optical intensity. In fact, Helmholtz's equation, in its generality, describes both beams and their interaction, which in nonlinear optics is two-fold: the standard coupling due to refractive index inhomogeneity and the refractive index dependence on each single intensity.

The complex amplitude $\mathbf{E}_\omega(\mathbf{r})$ of the monochromatic optical field $\mathbf{E}(\mathbf{r},t) = \mathrm{Re}(\mathbf{E}_\omega(\mathbf{r})e^{-i\omega t})$ is correctly described by Helmholtz equation

$$\nabla^2\mathbf{E}_\omega + k_0^2 n^2 \mathbf{E}_\omega = 0\,, \tag{5.1}$$

where $k_0 = \omega/c$, and n is the total refractive index which we will assume to be of the form

$$n = n' + \Delta n(\mathbf{r})\,, \tag{5.2}$$

$n' = n_0 + i\alpha$ being the unperturbed refractive index of the crystal and $\Delta n(\mathbf{r})$ its small variation due to photorefractive effect ($\Delta n \ll n_0$). Generalizing the slowly-varying amplitude approximation to the case of two counterpropagating beams, we look for an optical field of the form

$$\mathbf{E}_\omega(\mathbf{r}) = \mathbf{A}^{(+)}(\mathbf{r})e^{-i\beta z} + \mathbf{A}^{(-)}(\mathbf{r})e^{-i\beta z}\,. \tag{5.3}$$

On substituting Eq. (5.3) in Eq. (5.1) and with the approximation $n^2 \cong n'^2 + 2n'\Delta n$, we obtain the equation

$$\begin{aligned}&\left\{\left[\nabla_\perp^2 + \frac{\partial^2}{\partial z^2} + 2i\beta\frac{\partial}{\partial z} + 2ik_0^2 n_0\alpha + 2k_0^2(n_0 + i\alpha)\Delta n\right]\mathbf{A}^{(+)}\right\}e^{i\beta z} \\ &+ \left\{\left[\nabla_\perp^2 + \frac{\partial^2}{\partial z^2} - 2i\beta\frac{\partial}{\partial z} + 2ik_0^2 n_0\alpha + 2k_0^2(n_0 + i\alpha)\Delta n\right]\mathbf{A}^{(-)}\right\}e^{-i\beta z} = 0\,,\end{aligned} \tag{5.4}$$

where $\beta = k_0\sqrt{n_0^2 - \alpha^2}$ and $\nabla_\perp^2 = \partial^2/\partial x^2 + \partial^2/\partial y^2$. The paraxial approximation now consists in neglecting the $\partial^2/\partial z^2$ terms.[32] The resulting equation is satisfied on setting

$$\begin{aligned}\left[\frac{1}{2k}\nabla_\perp^2 + i\frac{\partial}{\partial z} + i\gamma\right]\mathbf{A}^{(+)} &= -\frac{k}{n_0}\Delta n\mathbf{A}^{(+)}\,, \\ \left[\frac{1}{2k}\nabla_\perp^2 - i\frac{\partial}{\partial z} + i\gamma\right]\mathbf{A}^{(-)} &= -\frac{k}{n_0}\Delta n\mathbf{A}^{(-)}\,,\end{aligned} \tag{5.5}$$

where $k = k_0 n_0$, $\gamma = k_0^2 n_0\alpha/\beta$ and we have used the fact that $\beta \cong k$ (we have also neglected α with respect n_0 in the r.h.s. of (5.5)).

In what follows we formulate the problem in more general context, introducing, along with the diffusive nonlinearity, also drift contributions in the form of a screening term, underlining the fact that, as previously mentioned, the experimental realization of a counterpropagating configuration with a constant value of background illumination I_b introduces a relevant experimental complication (whereas in the mere diffusive nonlinearity this problem does not arise). In centrosymmetric photorefractive media, the expression of the Δn as a function of optical intensity is (see Eqs. (2.2), (3.2) and (3.3))[27]

$$\Delta n = -(1/2)n_0^3 g\varepsilon_0^2(\varepsilon_r - 1)^2 \left[-\frac{K_B T}{q}\frac{d}{dx}\log\left(\frac{I + I_b}{I_b}\right) + \frac{w}{I + I_b}\right]^2 , \tag{5.6}$$

where $I = |\mathbf{A}^{(+)}e^{i\beta z} + \mathbf{A}^{(-)}\mathbf{e}^{-i\beta z}|^2$ is the optical intensity, and w is a constant that depends on the bias voltage. Expression (5.6) works under a number of approximations one of which, namely $|\partial I/\partial z| \ll |\partial I/\partial x|$, forces us to consider mutually incoherent beams whose total optical intensity is $I = |A^{(+)}|^2 + |A^{(-)}|^2$; besides, expression (5.6) is valid only in the 1+1D case. The "free" parameters w, I_b, ε_r, testify to the high degree of tunability of the centrosymmetric near-transition interaction. Other degrees of freedom come from the choice of the boundary conditions

$$\begin{aligned} A^{(+)}(x,0) &= f^{(+)}(x)\,, \\ A^{(-)}(x,L) &= f^{(-)}(x)\,, \end{aligned} \tag{5.7}$$

where L is the crystal length in the propagation direction z.

Equations (5.5) are the fundamental, coupled, parabolic, equations describing counterpropagating beam interaction. We stress that beam-coupling comes only from refractive index dependence on both beam intensities: beam-interaction from index-inhomogeneity may be neglected whenever Δn is a slowly varying function of z, and this is the limit in which our scheme works. As mentioned, an interesting feature of each beam propagation contained in Eqs. (5.5) is nonlocal optical-feedback. Let us consider $A^{(+)}$: it starts its propagation in a refractive index locally depending on $A^{(-)}$ which in turn propagates from $z = L$ self-consistently affected by $A^{(+)}$ in other points of the crystal. So $A^{(+)}$ is indirectly affected in its propagation by its shape in more than one point of the medium and this is precisely an optical-feedback effect. In a particular symmetric condition, such a feedback effect is more evident. Suppose, for example that $f^{(+)}(x) = f^{(-)}(x)$, true if beams entering opposite sides of the crystal are identical; one can show in a straightforward manner, starting from Eq. (5.5), that $A^{(-)}(x,z) = A^{(+)}(x, L - z)$ inside the whole crystal. Inserting this relation in the first equation of (5.5) we obtain

$$\begin{aligned} \left[i\frac{\partial}{\partial z} + \frac{1}{2k}\frac{\partial^2}{\partial x^2} + i\gamma \right] A^{(+)} &= -\frac{kn_0^2 g\varepsilon_0^2(\varepsilon_r - 1)^2}{2} \\ &\quad \times \left[-\frac{K_B T}{q}\frac{d}{dx}\log\left(\frac{I + I_d}{I_d}\right) + \frac{w}{I + I_d}\right]^2 A^{(+)}\,, \\ I(x,z) &= |A^{(+)}(x,z)|^2 + |A^{(+)}(x, L - z)|^2\,, \end{aligned} \tag{5.8}$$

which is a single equation for $A^{(+)}$, completely equivalent to Eq. (5.5). Feedback and strong nonlocality is manifested in the direct dependence of $A^{(+)}$ at (x, z) on $A^{(+)}$ at $(x, L - z)$. This formally closes the head-on collision problem.

Mathematical difficulties in handling Eq. (5.5) (or Eq. (5.8) in symmetric condition) lead us to adopt a numerical scheme. Moreover, having in mind the realization of versatile optical devices, we are forced to use a method capable of predicting, at least in principle, optical field behavior inside the crystal *for a general set of external parameters and boundary conditions.* The numerical method we use in solving Eq. (5.5) with conditions (5.7) is based on an iterative scheme. At the first step we introduce in expression (5.6) a two test functions $A_0^{(+)}$ and $A_0^{(-)}$ satisfying (5.7) (they may be, for example, free fields) and we solve Eq. (5.5) (which now are two linear partial differential equations) with the method of finite differences, obtaining two functions $A_1^{(+)}$ and $A_1^{(-)}$ (imposing (5.7) on them). At the second step we introduce $A_1^{(+)}$ and $A_1^{(-)}$ in (5.6) and in Eq. (5.5), obtaining an expression for $A_2^{(+)}$ and $A_2^{(-)}$. It can be shown that upon iterating, the sequence of $A_n^{(+)}$ and $A_n^{(-)}$ converges to the solutions $A^{(+)}$ and $A^{(-)}$ of (5.5). The sequence is truncated when conditions $A_{n-1}^{(+)} \cong A_n^{(+)}$ and $A_{n-1}^{(-)} \cong A_n^{(-)}$ are fulfilled (within the chosen accuracy).

Acknowledgement

The work of E. DelRe was carried out in the framework of an agreement between the Fondazione Ugo Bordoni and the Italian Telecommunications Administration.

References

1. For an exhaustive overview and bibliography on the subject, see A. Degasperis, *Am. J. Phys.* **66**, 486 (1998).
2. For an accessible introduction, and bibliography, to conventional integrable systems supporting solitons, like the nonlinear-Schroedinger-Equation supporting optical temporal solitons, see P. Drazin and R. Johnson, in *Solitons: an Introduction* (Cambridge University Press, Cambridge, 1989).
3. M. Segev and G. I. Stegeman, *Physics Today*, August 1998.
4. M. Segev, G. Valley, B. Crosignani, P. Di Porto and A. Yariv, *Phys. Rev. Lett.* **73**, 3211 (1995); for an up-to-date review, see Ref. 27.
5. M. Shih, M. Segev, G. Valley, G. Salamo, B. Crosignani and P. Di Porto, *Electron. Lett.* **31**, 826 (1995).
6. M. Shih, M. Segev and G. Salamo, *Phys. Rev. Lett.* **78**, 2551 (1997).
7. M. Mitchell and M. Segev, *Nature* (London) **387**, 880 (1997).
8. M. Segev, B. Crosignani, A. Yariv and B. Fischer, *Phys. Rev. Lett.* **68**, 923 (1992).
9. A. Agranat, V. Leyva and A. Yariv, *Opt. Lett.* **14**, 1017 (1989).
10. B. Pesach, E. Refaeli and A. Agranat, *Opt. Lett.* **23**, 642 (1998).
11. A. Agranat, R. Hofmeister and A. Yariv, *Opt. Lett.* **17**, 713 (1992).
12. M. Segev and A. Agranat, *Opt. Lett.* **22**, 1299 (1997).
13. E. DelRe, B. Crosignani, M. Tamburrini, M. Segev, M. Mitchell, E. Refaeli and A. Agranat, *Opt. Lett.* **23**, 421 (1998).
14. E. DelRe, M. Tamburrini, M. Segev, E. Refaeli and A. Agranat, *Appl. Phys. Lett.* **73**, 16 (1998).

15. G. Valley *et al.*, *Phys. Rev.* **A50**, R4457 (1994).
16. B. Crosignani, E. DelRe, P. Di Porto and A. Degasperis, *Opt. Lett.* **23**, 912 (1998).
17. B. Crosignani, A. Degasperis, E. DelRe, P. Di Porto and A. J. Agranat, *Phys. Rev. Lett.* **82**, 1664 (1999).
18. Y. Xu, in *Ferroelectric Materials and Their Applications* (North-Holland, Amsterdam, 1991).
19. K. Kos *et al.*, *Phys. Rev.* **E53**, R4330 (1996).
20. In *Photorefractive Materials and Their Applications I*, eds. P. Gunter and J.-P. Huignard (Springer-Verlag, Berlin, 1988).
21. M. Segev, M. Shih and G. Valley, *J. Opt. Soc. Am.* **B13**, 706 (1996).
22. F. Jona and G. Shirane, in *Ferroelectric Crystals* (Dover, New York, 1993).
23. A. Zozulya *et al.*, *Europhys. Lett.* **36**, 419 (1996).
24. B. Crosignani *et al.*, *J. Opt. Soc. Am.* **B14**, 3078 (1997).
25. M. Saffman and A. Zozulya, *Opt. Lett.* **23**, 1579 (1998).
26. S. Gatz and J. Herrmann, *Opt. Lett.* **23**, 1176 (1998).
27. B. Crosignani, P. Di Porto, M. Segev, G. Salamo and A. Yariv, *La Rivista del Nuovo Cimento* **21–6** (1998).
28. For an introduction to photorefraction, see P. Yeh, in *Introduction to Photorefractive Nonlinear Optics* (Wiley, New York, 1993).
29. E. DelRe, A. Ciattoni, B. Crosignani and M. Tamburrini, *J. Opt. Soc. Am.* **B15**, 1469 (1998).
30. A. Yariv and P. Yeh, in *Optical Waves in Crystals* (Wiley, New York, 1984).
31. L. Solymar, D. J. Webb, A. Grunnet–Jepsen, in *The Physics and Applications of Photorefractive Materials* (Clarendon Press, Oxford, 1996).
32. A. Yariv, in *Optical Electronics*, 4th Edition (Oxford Press, New York, 1991).